Wood Science and Technology (2025) 59:24
https://doi.org/10.1007/s00226-024-01622-6

ORIGINAL

# Morphological analysis of inosculated connections in weeping figs: insights on density, geometry, fiber structures, and compositional variations

**Xiuli Wang[1,2] · Wolfgang Gard[1] · Yasmine Mosleh[1] · Jan-Willem van de Kuilen[1,3]**

Received: 23 July 2024 / Accepted: 13 November 2024 / Published online: 16 January 2025
© The Author(s) 2024

## Abstract

Trees exhibit adaptability in response to external loads, which allows them to form an inosculated connection (self-growing connection) with a neighboring tree. Such connections have the mechanical potential to build living tree structures. Although qualitative studies have studied this phenomenon, quantitative analysis of its growth features remains limited. Self-growing connections fused by weeping figs (*Ficus benjamina* L.) are utilized to study growth features. X-ray scanning and optical microscopy techniques are employed to investigate parameters including density, geometry, fiber structures, and material compositions. Key findings demonstrate that the fused region of a connection has a larger volume and a higher density on the intersected surface. Microscopic analysis identifies that the enlarged wood in the fused area is tension wood characterized by G-layers. The key component that connects trees is referred to as merged fibers, and the pattern of their distribution is found to be mainly in the outer layer of the larger cross-angle of a connection. At the cellular level, crystals within cells are identified in the fused region, implying possible mechanical stresses the interface has experienced. The findings in self-growing connections can serve as inspiration for structural design in living structures, biomimicry, bioinspired structures, and advancements in bioeconomics.

## Introduction

In nature, trees can grow adaptively in response to external loads, which allows them to form an inosculated connection with a neighboring tree, e.g., connections in Figs. 1a and b (Jaffe 1980; Mattheck 1997; Ludwig et al. 2019; Wang et al. 2020). This connection is termed the self-growing connection in this research, which highlights its natural ability to grow and optimize its morphology (Wang et al. 2020). Self-growing connections have the potential to be used as basic structural elements to construct living structures (e.g., Fig. 1c). Although the concept of applying living structures is gradually gaining attention, such as living pavilions, living root bridges,

Extended author information available on the last page of the article

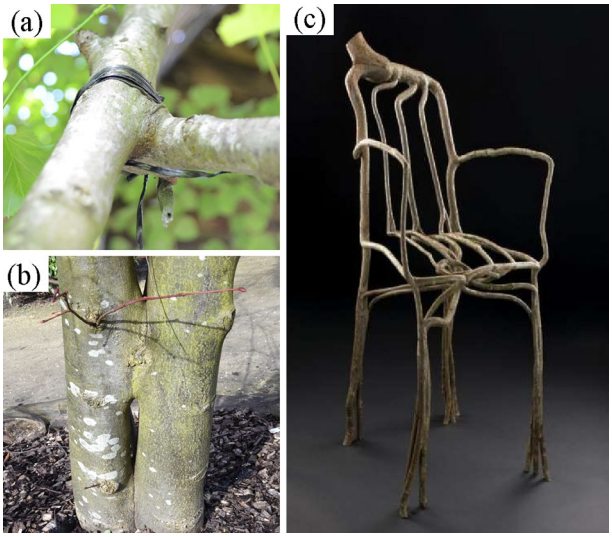


**Fig. 1** Self-growing connections and living structures. The cross (**a**) and parallel (**b**) self-growing connections fused by lime trees; (**c**) a chair naturally grown from willow trees; photo credits: Full Grown, UK

and Baubotanik (Ludwig et al. 2012, 2019; Shankar 2015; Wang et al. 2020), to the best knowledge of the authors, there is a lack of quantitative understanding and evaluation methods regarding the load-carrying capacity of the formed structures. However, the growth characteristics need to be known before investigating the mechanics of self-growing connections.

As in Fig. 1, lime (*Tilia cordata*) (Wang et al. 2020), willow (*Salix alba*) (Ludwig et al. 2012; Mylo et al. 2021) and fig (*Ficus elastica*) (Shankar 2015) can fuse in stems, branches, and roots to form connections. The formation speed depends on the growth rate of the tree species, among which *Ficus* is a relatively fast-growing tree species (Scuderi et al. 2012; Shankar 2015). Furthermore, it has the feasibility to create connections in nurseries; thus, it is suitable for performing laboratory research. The principle of the grafting or fusion technique is to fuse the cambium layers of trees, from which new tissues grow and develop for the connectivity (Millner 1932; Brown and Sax 1962; Melnyk 2017). The mechanism of adaptive growth can be understood as the morphological optimization in the stressed region under loads (Telewski and Jaffe 1986; Braam 2005; Hamant et al. 2008; Hamant and Traas 2010; Coutand 2010; Moulia et al. 2015). The outcome is that a tree minimizes resource usage during growth, while effectively mitigating stress and deformations in high-stress regions for optimal loading performance. The changes that occur in this process can be described in four aspects, namely density distributions, geometric changes, fiber structures, and anatomical composition (Telewski and Jaffe 1986; Hamant et al. 2008; Moulia et al. 2015; Hamant and Moulia 2016).

Wood density is widely considered to vary linearly with wood stiffness and strength (Chave et al. 2009; Niklas and Spatz 2010). Geometric changes resulting

from adaptive growth usually develop asymmetric shapes around the growth axes (Fournier et al. 2013). Additionally, the accumulation of wood is accompanied by the production of reaction wood and changes in fiber structures (Wardrop and Dadswell 1948; Kouhen et al. 2023). For example, in response to wind-induced bending, trees decrease the length to slenderness ratio of their stems and develop an oval cross section (Nicoll and Ray 1996; Danjon et al. 2005). Deciduous trees form tension wood on their tensioned side (Zimmermann et al. 1968). Similarly, studies on tree branch connections (Slater and Ennos 2013, 2015; Özden et al. 2017) suggest that the joint region exhibits higher density and interlocking fiber patterns, which enhances the safety of the tree structure. At the microscopic scale, the nonuniform distribution of density, and changes in geometry and fiber direction result from variations in cell morphology and tissue organizations. For instance, tension wood is considered superior tensile strength compared to normal wood due to more cellulose content, and it can be distinguished by G-layers (gelatinous fibers) within cell walls in anatomy (Wardrop and Dadswell 1948; Côté et al. 1969; Clair et al. 2006).

Regarding the techniques for measurements, X-ray computer tomography (CT) scanning is frequently utilized to characterize wood density and geometry in trees (Freyburger et al. 2009; Tanaka and Kawai 2013; Mylo et al. 2021). The acquired image data enables analysis to determine the relative distribution of density and to compare sizes across different slices, while minimizing damage on connections. In anatomical analysis of wood, optical microscopy is commonly employed (Siddiqi 1991). Regarding hardwood species, the observations focus on identifying the morphology and direction of fiber, ray, vessel, and parenchyma cells.

Therefore, this paper investigates characteristics of self-growing connections fused by weeping figs (*Ficus benjamina* L.) in four aspects (density, geometry, fiber structures, and anatomical compositions) using CT scanning together with optical microscopy. Understanding of the characteristics of a self-growing connection is part of systematic studies in Wang (2024), and it serves not only to predict its mechanical potential, but also to draw inspiration from natural structures for application in engineering structures, such as bioinspired and biomimicry design.

## Materials and methods

### Braided weeping figs and self-growing connections

In this study, self-growing connections fused by weeping figs (*Ficus benjamina* L.) were prepared. An example of the braided tree structure can be seen in Fig. 2a. The diameter of the braided net was measured between the outermost distance, and the height was measured from the base of the stem to the location of the last connection. Three braided figs (Tree T, Tree B, and Tree S) with different net sizes were prepared and are recorded in Table 1.

To have a standard comparison among different connections, a unified description was made. As in Fig. 2b, a local coordinate system was placed at the intersection of the central lines of two stems (stem1 and stem2). The cross angle of the connection was measured as the relatively small angle ($\alpha$) between two stem central lines. The

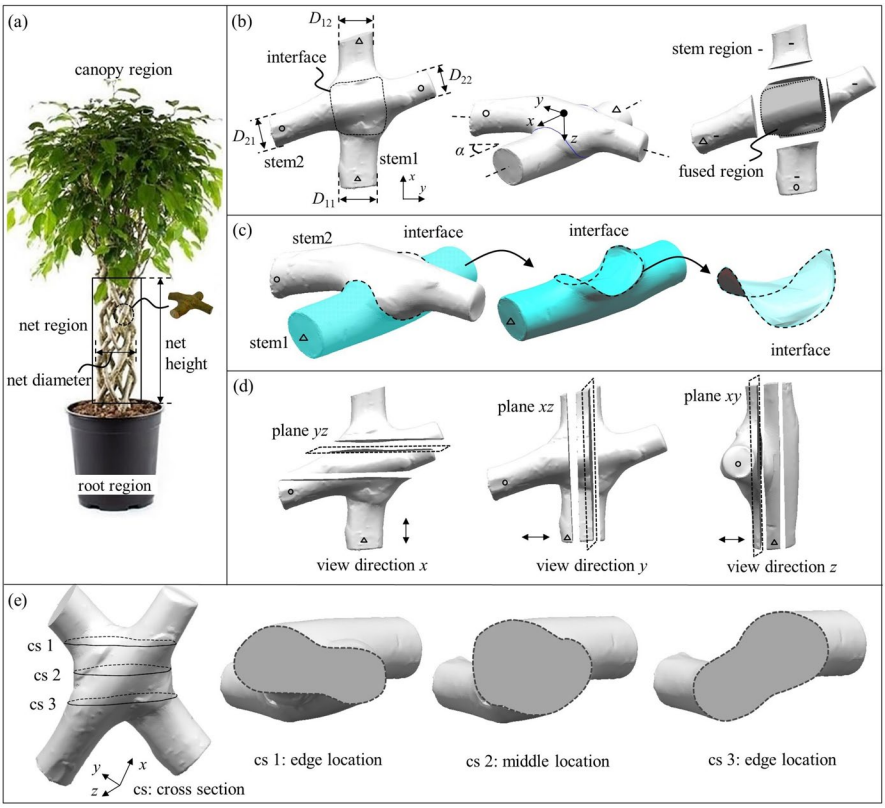


**Fig. 2** Descriptions of braided tree structures and self-growing connections. (**a**) An example of braided tree structures. (**b**) Geometric illustrations of self-growing connections, including different regions (stem and fused regions), diameters ($D_{11}$, $D_{12}$, $D_{21}$, and $D_{22}$), and cross angle ($\alpha$). (**c**) 3D saddle shaped interface outlined by the bark edge of two stems. (**d**) According to the coordinate in (**b**), a connection can be viewed in three anatomical directions, view directions in $x$, $y$, $z$ axes respectively. (**e**) Cross-sectional appearance at the edge and middle locations within a connection

**Table 1** Geometric information on braided tree structures for tests

| ID | Net region (mm) | | Number of stems | Number of connections | Average stem diameter (mm) |
|---|---|---|---|---|---|
| | Diameter | Height | | | |
| Tree T (Tr_T, TT) | 200 | 800 | 8 | 24 | 20.3 |
| Tree B (Tr_B, TB) | 160 | 900 | 8 | 32 | 19.0 |
| Tree S (Tr_S, TS) | 120 | 600 | 8 | 28 | 14.6 |

$x$ axis was aligned with the direction of the relatively larger stem (stem1). The connection was divided into stem and fused regions based on the interface, which was distinguished by the boundary between the barks and formed a three-dimensional shape like a saddle, as in Fig. 2c. Unlike anatomical observations of wood in three

sections (transverse, radial, and tangential), the cross section of a self-growing connection, especially in the fused region, consisted of two different sections from two stems. Therefore, the anatomical directions of self-growing connections were categorized into three types based on the local coordinate plane, as shown in Fig. 2d. For example, in the view direction of axis $x$, the cross sections were cut in the plane $yz$ and each section contained a transverse cut of stem1 and a clip cut of stem2. Similarly, in view directions $y$ and $z$, the section of a connection consisted of a longitudinal cut of stem1, and a clip cut of stem2.

During the growth of a connection, the amount of fused material may vary in different areas because of the developmental sequence of growth. Within the fused region, it can be assumed that the fusion activity first occurs at the center of the connection, where two stems have earliest contact and it experiences the longest time for growth. This is assumed to have a high fusion level. In contrast, towards the periphery of the fused region, particularly at the edges, the degree of fusion is comparatively lower and occurs later. To be specific, as presented in Fig. 2e, in the cross-sectional area near the center of the fused region (cs 2), the fusion level is considered high. Under this condition, the cross section exhibits an approximately circular shape. In contrast, toward the edges of the fused region (cs1 and cs3), where the fusion level is considered lower, the cross-sectional shape exhibits an overlap of the transverse sections of the two stems and has a gourd-like shape. Additionally, the distance between the two trees' piths is greater compared to cs2. After the basic description of the connections is presented, they are prepared for measurements. All connections were in fresh condition when they were tested.

### Characterization of density variations using calibrated CT

The density variation within a connection was inspected non-destructively by the calibrated computer tomography (calibrated CT) scanner (Siemens Somatom Volume Zoom CT scanner, Germany). The Hounsfield value of the scanner at −1000 was calibrated with air density (apply 0 kg/m$^3$), and the value at 0 was calibrated with water density (1000 kg/m$^3$). Following the method implemented in Freyburger et al. (2009), the obtained scanning was linearly calibrated. Thus, the linear calibration function can be expressed as Eq. 1

$$\rho = h + 1000, \tag{1}$$

where $h$ stands for the Hounsfield value of CT scanning, $\rho$ is the corresponding material density, in kg/m$^3$. The density refers to the density of the material of living trees. The braided trees were scanned only within the net region, and the results were constructed from slices at 0.6 cm intervals with a resolution of 0.6 mm. The calibration and analysis of the density variations were performed by ImageJ.

### Characterization of geometric changes using calibrated CT

From the scanning results in Sect. "Characterization of density variations using calibrated CT", as shown in Fig. 3, the geometric variation within the braided tree

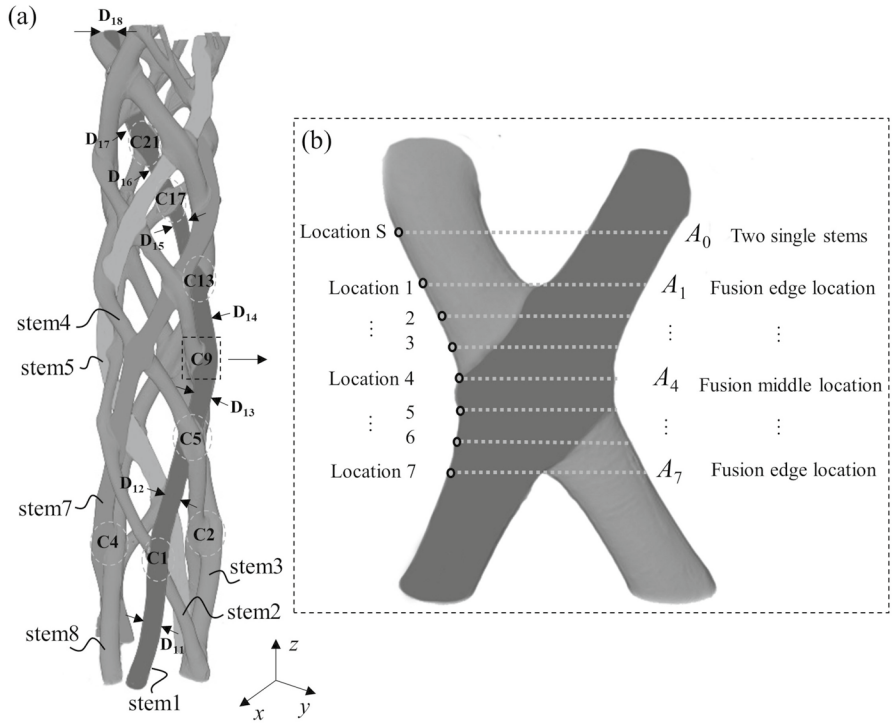


**Fig. 3** Illustration of geometric measurements on the braided tree structure and self-growing connections. (**a**) Within a braided tree structure, the denotations of stems, connections (C) and measured intervals. Diameters (*D*) of each stem between connections are measured, e.g., diameter of stem1 in the first interval is $D_{11}$. (**b**) Within a self-growing connection, the area comparison between the cross section in the stem and fused region. Locations 1 and 7 are taken at the edge location in the fused region, whereas the other five locations are uniformly taken in between. Note: $A_i$ is area of a cross section in the fused region, *i* from 1 to 7; and $A_0$ is area of a cross section in the stem region

structure was measured at two levels, namely at the level of the braided tree structure and at the connection level. The first level of measurement was to understand and compare the variation of diameters caused by the presence of connections in a braided tree structure. The second was to further measure the changes in geometry within a connection caused by the fusion activity.

The geometric measuring approaches for tree structures and within a connection are shown in Fig. 3. Measurements along each stem were made at the midpoint of each interval between neighboring connections, avoiding the presence of knots, branches, and other defects (such as uneven surfaces); the average value was made from three measurements. The taper ratio of a stem was calculated by the ratio between the top diameter and the base diameter of a stem. For example, the tapering ratio of stem1 was the ratio between $D_{18}$ and $D_{11}$ in Fig. 3a.

Quantification of geometric changes within a connection was achieved by comparing area variations at several spatial locations in the stem region and the fused region. In the same viewing direction (along the vertical growth direction of the tree

structure), within the fused region, a total of seven locations were chosen uniformly (Fig. 3b). The area of each cross section was measured using ImageJ. The mean value of measurements was calculated by averaging values of two adjacent slices at each location. The area in the fused region was further compared with the area in the stem region which was measured below the connecting point to exclude the possible influence from tapered stems. To ensure comparability of the results across connections, the difference between the fused and stem regions was normalized by the area within the stem region. The area difference was further divided by the area in the stem region. Thus, the obtained ratio could be used to compare connections. This ratio was defined as the over-grown ratio ($r$). The formula is expressed in Eq. 2.

$$r = \frac{A_i - A_0}{A_0}, \tag{2}$$

where $A_i$ is the area of a cross section in the fused region, $i$ from locations 1 to 7; and $A_0$ is the area of a cross section in the stem region. In total, 27 connections were measured in the braided tree structure Tree B and 16 connections in Tree S. The information about braided tree structures is listed in Table 1.

### Characterization of fiber structures using Micro CT

The internal fiber structures of a connection were inspected by Micro CT scanning (Phoenix Nanotom, 180 kV, 0.5 mA, with a resolution of 60 µm). In total, 12 connections were taken from three trees. In Tree T, the selected connections included C1, C2, C4, C5, and C8. In Tree B, the selected connections included C4, C5, C8 and C17. In Tree S, the selected connections included C1, C6, and C12. The reconstructed scanning results were inspected from three view directions, as illustrated in Fig. 2d. This inspection focused on the fiber patterns within a connection.

### Characterization of anatomical compositions using optical microscopy

In the stem region, the anatomy was inspected in transverse, tangential, and radial sections. In the fused region, a connection was cut into several partitions in the fused region. In the viewing direction of $y$, the fused region was uniformly divided into six zones. Similarly, in the $x$ viewing direction, six partitions were made evenly. Since in the $z$ direction, the width of the fused region was relatively small, the fused region of a connection was uniformly divided into four parts. The thickness of each partition was determined to be approximately 5 mm, and at least five slices for anatomical observations were made in each partition. In total, 15 self-growing connections from braided Tree B (C5 – C19) and 15 connections from Tree S (C5 – C19) were chosen and cut for inspection. For three different evaluation directions, these connections were further separated into three groups. It had ten connections from each braided tree in each group. Glass slides for microscopic investigations were prepared according to the instructions (Tardif and Conciatori 2015). Table 2 presents sample information for the slides.

**Table 2** Information on the preparation of microscopic slices in a self-growing connection

| Stem (40 samples) | | Connections (10 samples in each direction) | | | |
|---|---|---|---|---|---|
| Cross section | Slice thickness (μm) | View direction | Partition | Slice thickness (μm) | Number of slices in each partition |
| Transverse | 20 | *x* direction | 6 | 35 ~ 45 | 8 |
| Radial | 20 | *y* direction | 6 | 35 ~ 45 | 8 |
| Tangential | 20 | z direction | 4 | 50 ~ 60 | 5 |

After the slices were prepared, they were rinsed and dehydrated by a series of ethanol solutions (50%, 70%, and 90%) and then fixed to microscopic glasses. The optical microscope (Keyence VHX7000, Germany) was used at magnifications from 20 × to 2000 × for characterizations at different resolutions. The analysis was run using Keyence communication software. Anatomical characteristics were studied and quantified using the IAWA approach (IAWA Committee 1989).

## Results

### Density variations

The results of Tree T are used as a representative, and results of the other two trees can be found in the supplementary information (Figs. S1 and S2). Two representative slices (Tr_T_lc1 and Tr_T_lc2) were selected from the scanned results to analyze in Fig. 4a. The first selection (Tr_T_lc1) contained the middle fusion locations of four connections (Fig. 4b). The second selection (Tr_T_lc2) contained the stem section, edge fusion, and middle fusion to compare (Fig. 4c). To better highlight regions with higher density, two threshold values were established at 400 and 1000 kg/m$^3$. In Fig. 4c, the histogram of the Hounsfield value of the square area in C13 is presented as an example.

Materials with higher density were distributed mainly in the outer layer and the inner fused area (Fig. 4b and d) in cross sections. The outer layer was recognized as the bark area. On the contrary, the inner stem region has a relatively lower density of less than 1000 kg/m$^3$. However, in the region pointed out by arrows, a contiguous area of density (in light blue) was observed, representing the wood of the stem. When comparing the edge fusion in Fig. 4d (C2 and C3), the density distribution appeared as a combination of two single stems. On the contrary, at the middle location of the fusion region (C14 and C15 in Fig. 4b, C1 in Fig. 4d), where the fusion level was assumed to be higher, the density distribution was observed to have a contiguous area in the cross section pointed at by arrows.

The results of Fig. 4d were further analyzed by line probing that passed through the stem region, the two edges of the fused region, and the central location of the fused region. On a single stem (line1 in Fig. 4e), the density of the wood could be considered relatively homogeneous. The intersected regions in Fig. 4d, which were

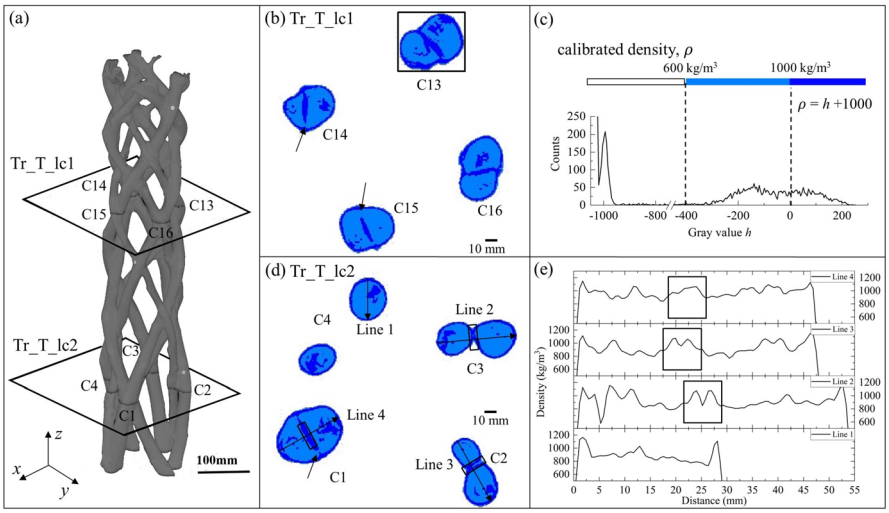


**Fig. 4** Density distributions within Tree T at two locations (Tr_T_lc1 and Tr_T_lc2). (**a**) Indication of the inspected locations in the Tree T; (**b**) density map at location Tr_T_lc1 in (**a**); (**c**) histogram of gray value distributions within the rectangular area in C13 in (**b**), where the color map of calibrated density is indicated; (**d**) density map at location Tr_T_lc2 in (**a**). (**e**) Density variations following probe lines in (**d**), where the square areas indicate the intersected areas in different fusion levels

marked in the rectangular area, the density profiles presented a hill-shaped region. However, at the edge of fused region in some area, as pointed out by the arrows, the interface showed a valley in the hill-shaped region in Fig. 4e. This observation was further identified as included in the bark gap in the anatomical compositions in Sect. "Relation between fiber structures and geometric variations".

## Geometric changes

In Fig. 5a and b, the influences of the formation of connections on the diameters along each stem are presented for Tree T. Fig. S3 gives information of Tree B and Tree S. The results showed that the maximum and minimum magnitudes of the diameters were observed between the connections rather than at the base or canopy locations of stems.

The taper ratio was not significant compared to the diameter difference caused by the formation of connections in the stems. Regarding single stem trees, the biomass allocation along the stem is generally considered different due to the growth of branches and the adaptive growth from self-weights. As a result, the overall shape of the stem is considered parabolic with the oldest cambium age in the basal area (Larson 1963). However, in studies (Larson 1963; Biondi 2020), it is also argued that in the growth of a branch-free stem, the distribution of wood in the stem is homogenous. In this study, the stems in the net region have no branch growth, if it is assumed that uniform growth is distributed along the stem when connections are not formed, the formation of connections influences diameter variations along

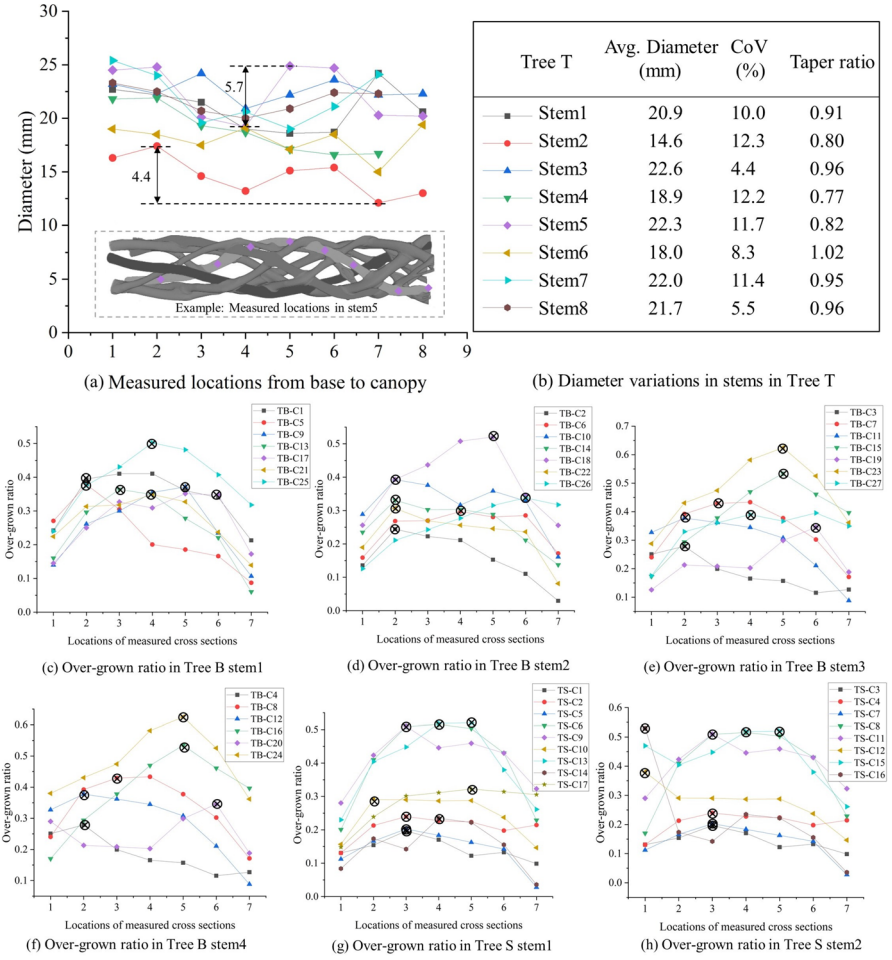


| Tree T | Avg. Diameter (mm) | CoV (%) | Taper ratio |
|---|---|---|---|
| Stem1 | 20.9 | 10.0 | 0.91 |
| Stem2 | 14.6 | 12.3 | 0.80 |
| Stem3 | 22.6 | 4.4 | 0.96 |
| Stem4 | 18.9 | 12.2 | 0.77 |
| Stem5 | 22.3 | 11.7 | 0.82 |
| Stem6 | 18.0 | 8.3 | 1.02 |
| Stem7 | 22.0 | 11.4 | 0.95 |
| Stem8 | 21.7 | 5.5 | 0.96 |

**Fig. 5** Diameter variations in Tree T and the analyzed over-grown ratios in connections. (**a**) Diameter variations at intervals as depicted in Fig. 3a; (**b**) the average (avg.) stem diameter and calculated taper ratio. (**c**) to (**h**) Over-grown ratios of connections in Tree B (TB) and Tree S (TS). Note: cross marks indicate the peak values for connections

stems. This assumption and observation may be interpreted based on the grain-flow analogy (Cramer and Goodman 1983; Foley 2001) and the pipe theory (Valentine 1985; Lehnebach et al. 2018). To be specific, the formation of connections within stems may affect the transport of water, nutrients, and plant hormones which influence growth. Therefore, the induced resistance in transport due to connections may result in hormone gradients within the area of connections, which may further affect the deposition of wood production.

The geometric changes within a connection (Fig. 5c to h) were compared by over-grown ratios as described in Sect. "Characterization of geometric changes using calibrated CT". The first observation was that the overgrown ratios were positive in all

connections. This concluded that the fused area produced more wood than the stem region within a self-growing connection. Second, when looking at the trend line of variation, the peak value most likely appeared in the middle region, where the fusion had high levels. The frequency of peak magnitudes occurring in the middle locations 2 to 4 had 60%. The over-grown wood in the fused region may be considered as tension wood due to the adaptive growth, which will be examined in Sect." Relation between fiber structures and geometric variations".

## Fiber structures

The understanding of fiber structures of self-growing connections was achieved by combining optical microscopic observations and results from CT scans, as seen in Fig. 6. Regarding fiber structures, three major observations can be identified.

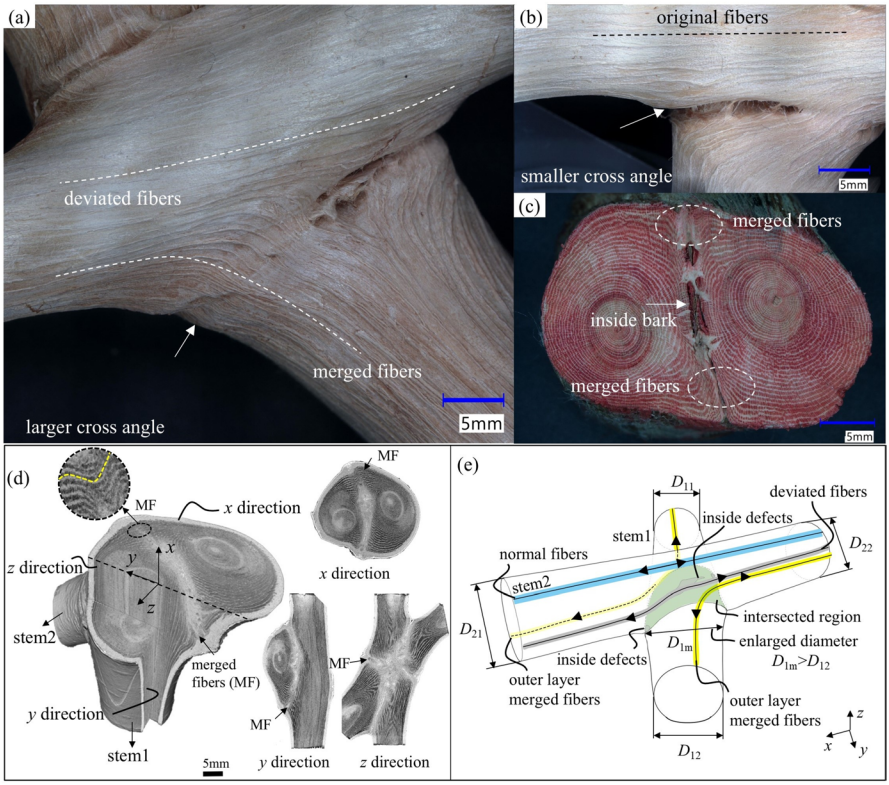


**Fig. 6** Fiber structures of self-growing connections under optical microscopy, CT scanning, and its conceptual model. Merged fiber bundles distributed in the outer layer (**a**) and in the smaller cross angle (**b**); (**c**) in the middle location within the fused region in *x* direction, few fiber bundles connect inside the connection. (**d**) Internal structures of a connection from X-ray scanning. (**e**) Conceptual fiber model of a connection

First, fiber bundles within a self-growing connection can be categorized into three groups based on their spatial distributions, namely original fibers, deviated fibers, and merged fibers, as shown in Fig. 6a, b, and c. The group of original fiber bundles formed independently in each stem without any influence of fusion activity (see Fig. 6b). In contrast, the deviated fibers, which located separately in each stem, were influenced by the fusion activity and resulted in deviation in their directions (see Fig. 6a). The merged fibers connected two stems together and produced at both stems. The direction of this group of fibers extended from one stem to another stem in a curved shape (see Fig. 6a). The change in fiber orientations of the deviated fibers could be explained similarly by the grain-flow analogy (Cramer and Goodman 1983; Foley 2001; Kramer 2002, 2006) as discussed in the Sect. of "Geometric changes".

Secondly, merged fibers were crucial for the formation and structural properties of a self-growing connection. The distribution pattern of this group of fibers was predominantly observed in the outer layer of a connection (Fig. 6a). From the results of CT scans, in the $x$ direction of the observed cross section, the merged fibers can be seen as continuous growth increments (Fig. 6d). Merged fibers were located at the larger cross-angle, while in the smaller cross-angle it showed the absence of the merged fibers (Fig. 6b). This might be that this optimized pathway via the larger cross angle minimizes the energy consumption for trees' growth and structural safety.

The third observation was that old bark tissues before the fusion were identified in Fig. 6b. As indicated in Hamant et al. (2008), the bark included before fusion still existed inside and new wood was produced on top of that after fusion. Moreover, little merged fibers are found inside a connection compared with the out-layer merged fibers. Figure 6d further shows three internal cross sections of the connection to support observations. Together with the findings in Sect. "Geometric changes", a conceptual fiber model was proposed to visualize observations (Fig. 6e). From Sect. "Geometric changes", it is concluded that the fused region had larger dimensions than at the stem region, which was also illustrated in Mattheck (1995).

### Relation between fiber structures and geometric variations

Because the production of wood is accompanied by the optimization of its fiber structures, the variations of over-grown ratios at different locations within the intersected region can be correlated with characteristics of fiber structures. Micro-CT scanned connections (C1, C2, C4, C5 and C8 in Tree T) were measured in the same way as in Fig. 3.

Internal structures of the Tree T (TT) C4 and TT-C8 are presented to explain the relation between fiber structures and geometric changes in Fig. 7. In connection TT-C4, the over-grown ratio peaked at the fourth measured location (Fig. 7a). Compared to the fourth location with the other locations (locations 2 to 5) in Fig. 7b, when the area reached the maximum value (location 4), the fiber structures showed the most fused fibers in the cross section. The same finding was identified in connection TT-C8 at location 3.

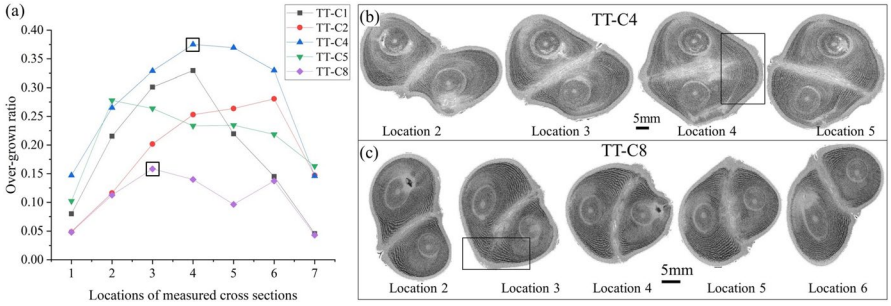


**Fig. 7** Area variations of Micro-CT scanned connections and internal structures. (**a**) Over-grown ratios in connections. (**b**) Cross-sectional appearance of C4 and C8 according to the measured locations in (**a**). The symbol TT-C indicates the connection in Tree T. The square area indicates the place having the most merged fibers

## Anatomical compositions

### Stem region

The wood of weeping figs was diffuse porous without distinct growth rings (Fig. 8). The growth increment consisted of axial parenchyma cells and fibers that alternated in pairs. In three cross sections (transverse, tangential, and radial) in Fig. 8c to e, the vessels of the weeping figs were circular or oval in outline and mostly solitary or some in a radial multiple of two to four in the transverse section. The fibers were square or polygonal in outline. The ray parenchyma cells were multi-seriate, which were mostly heterocellular and composed of procumbent cells and square cells. The axial banded parenchyma was present, and the cells were brick-shaped. Cell information obtained in the tree stem region of the tree was used to further identify cell types within the fused region, especially the orientation of the fiber.

### Fused region

In the fused region, for comparative analysis, the illustration included results from two sections: the edge of the fused region (the first partition in Table 2) in Fig. 9 and the middle of the fused region (the third and fourth partitions in Table 2) in Fig. 10. The tissues in the periphery of the fused region in the $x$ direction are shown in Fig. 9a and the slice made for this location is shown in Fig. 9b. The tissue organizations at this location are zoomed in in Fig. 9c. The interface at this location was found to consist primarily of bark tissues. The direction of the fibers was further identified. However, only parallel fibers were easily identified, marked as $F_{//}$. Inclined fibers ($F_a$) were mainly identified based on the appearance of the rays around them. Compared to the direction of the fiber in stem1, stem2, and the intersected region in Fig. 9b and c, when the fibers are close to

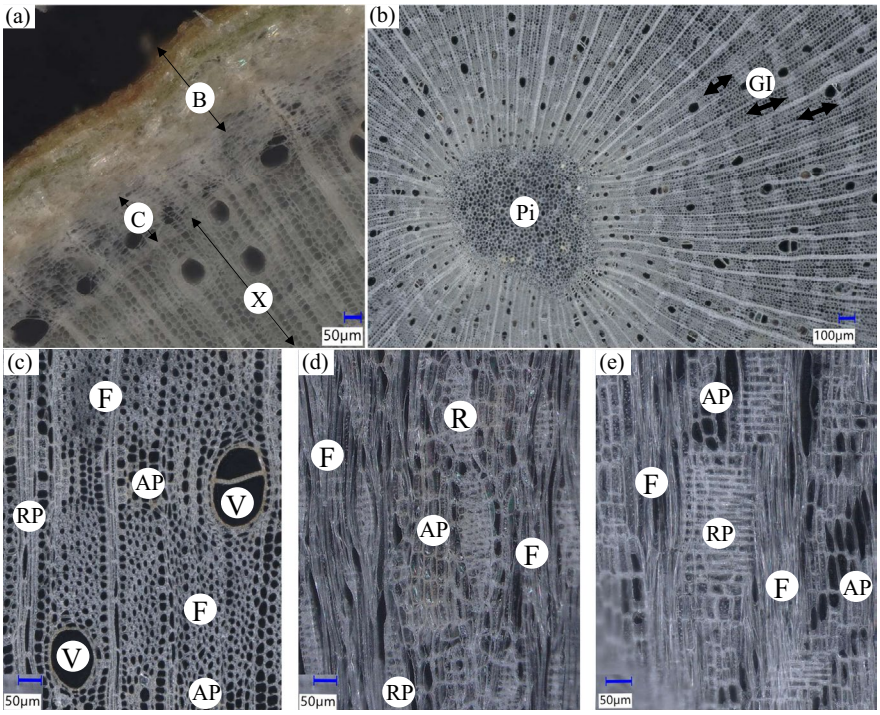


**Fig. 8** Anatomical overview of weeping figs in a cross-section of a stem, (**a**) in bark area and (**b**) in xylem (wood) region. Cross sectional appearance in xylem (**c**) transverse section; (**d**) tangential cross section; (**e**) radial section. Tissue types: bark (B), xylem (X), cambium zone (C), growth increment (GI), and piths (Pi). fibers (F), axial parenchyma cells (AP), ray parenchyma cells (RP), and vessel (V)

the interface, the direction of the fibers in stem1 changes from the perpendicular direction to the parallel direction gradually.

Figure S4 provides two other locations in the *y* and *z* directions to show how tissues connect and organize in the periphery locations. The locations presented correspond to the first partition in Table 2. Similarly to Fig. 9, the bark and parenchyma tissues made up the most connecting space at the intersection. A few fibers were spotted, but they are not continuously connected between two stems.

As shown in Fig. 10, four local areas were taken in the cross section and zoomed in for further research. In peripheral regions, tissues were observed to be continuously organized and free of flaws (Fig. 10c and f). The fibers that smoothly transferred from one stem to the other stem were marked by the dashed line. When comparing the outer locations (Fig. 10c and f) with the inner locations (Fig. 10d and e), the tissues in this inner region were less organized and the fiber bundles did not show a continuous merged pattern. Furthermore, this region was made primarily of bark parenchyma tissues. The results of the microanalysis at two locations in the fused region remained consistent with the observations in Sect. "Fiber structures".

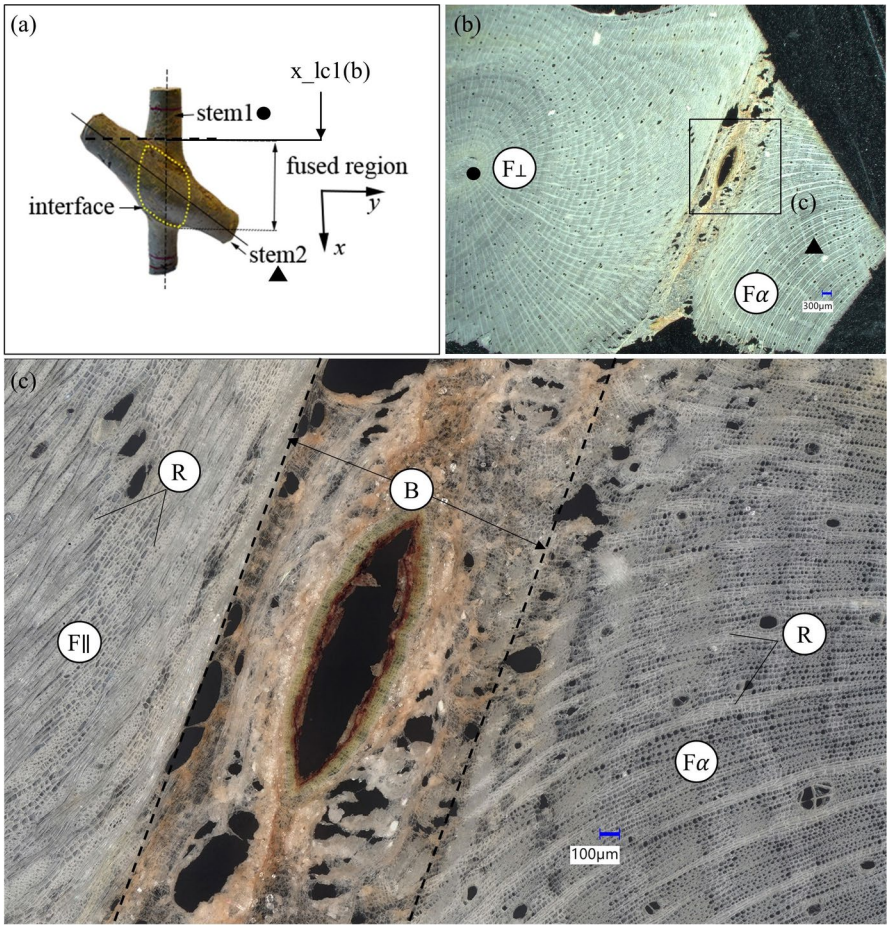


**Fig. 9** Tissue organization at the edge location of the fused region in *x* direction. (**a**) The inspection location (x_lc1) in a connection; (**b**) cross-sectional appearance of the inspected section, where the rectangular is magnified for further examination in (**c**). Tissue types: fibers (F), parenchyma cells (P), rays (R), and vessel (V). Parallel fibers are marked as $F_{//}$, inclined fibers are $F_{\alpha}$. The angle reference is the plane of the paper

## Cellular changes in the fused region

At the micro-scale, crystals in parenchyma cells were seen under the polarized light of the optical microscope in the fused interface within a connection (Fig. 11a and b). In addition to the crystals found at the interface, tension wood was also spotted according to the description in Ruelle (2014). Fiber cells with a G-layer were observed in the intersected area following the direction of the arrows (Fig. 11c and d). This finding proved that the enlarged volume within the fused region, as well as the fused fibers, was predominantly tension wood.

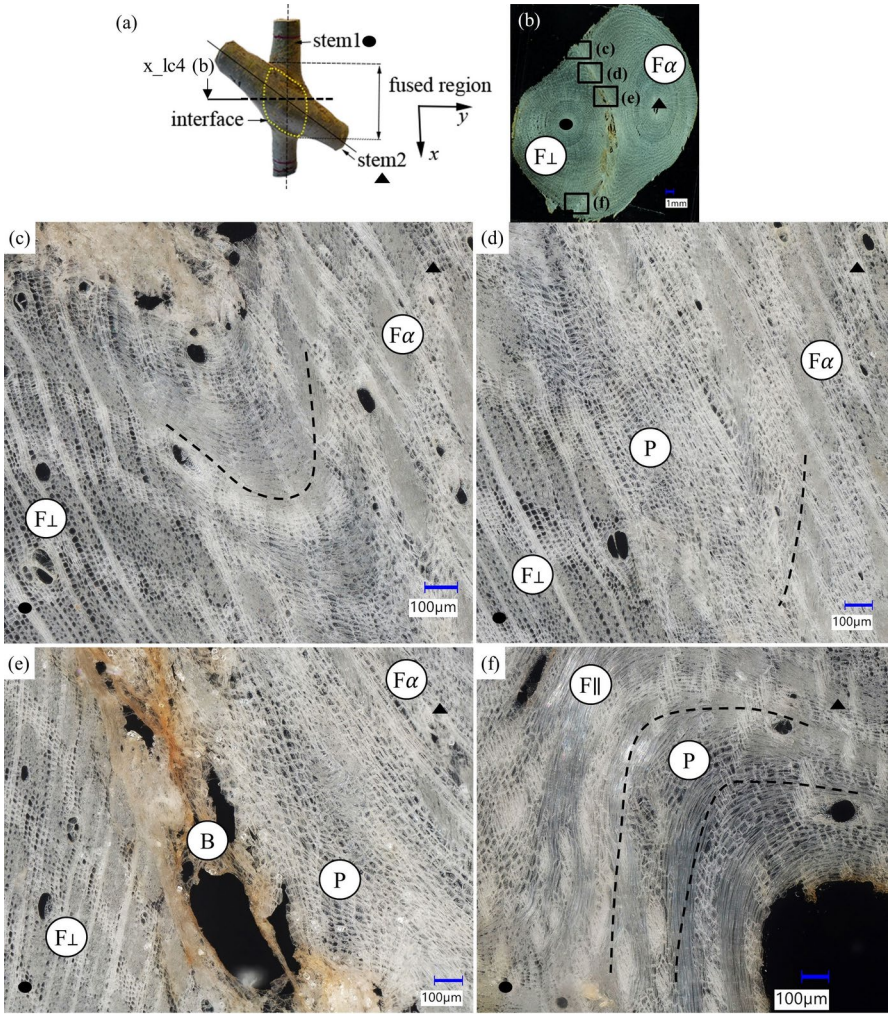


**Fig. 10** Tissue organizations at the middle location of the fused region in *x* direction. (**a**) The inspection location (x_lc4) in a connection; (**b**) cross-sectional appearance of the inspected section, where rectangular is magnified for further examination in (**c**), (**d**), (**e**) and (**f**). In the outer part in this cross section (**c**), (**d**), (**f**), more continuous merged fibers are spotted, but the inner part (e), mainly parenchyma cells are found. Tissue types: fibers (F), parenchyma cells (P), rays (R), and vessel (V). Parallel fibers are marked as $F_{//}$, perpendicular fibers are $F_{\perp}$, inclined fibers are $F_{\alpha}$. The angle reference is the plane of the paper

## Discussion

The implications of findings on mechanical applications are discussed in this section. High density and larger geometric dimensions may indicate high strength and stiffness in fused regions, according to studies (Chave et al. 2009; Niklas and Spatz 2010). The tension wood formed in the fused region also indicates the material's superior tensile strength (Clair et al. 2006). Regarding fiber structures, the crucial

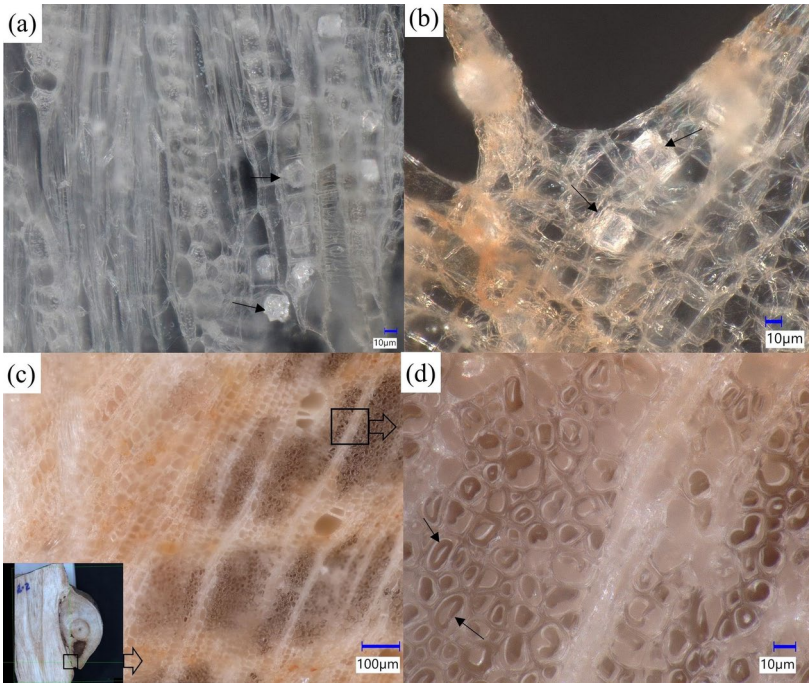


**Fig. 11** Changes occur in cells in the fused region. (**a**) and (**b**) Crystals identified in the fused region. Arrows point to the formed crystals. (**c**) Tension wood in the fused region. (**d**) The magnified region outlined by the rectangular in (**c**), arrows pointing to G-layers

component lies in the merged fibers. Their morphology and amount not only influence the fusion level but also predict the strength of the connection. As wood exhibits weaker strength in rolling shear and tension perpendicular to the grain direction compared to parallel (Van de Kuilen et al. 2017; Ehrhart and Brandner 2018), the distribution pattern of merged fibers indicates the potential weak areas in structural applications. The connection may be at risk of damage from tension and shear out of the interface. For example, considering the fiber structures in Fig. 6e, when the interface between the two stems is subjected to tensile forces, the merged fibers at the interface primarily resist the external load. The direction of these fibers is in a curved shape. Together with the saddle-shaped interface, the connected region has a complex stress environment under tension. At different points along the interface, variations in wood grain orientation lead to differences in the local material's load-bearing capacity. The overall load-bearing capacity of the interface can be understood as being controlled by the combination of the shear strength and the transverse tensile strength of the merged fibers.

In the intersected region, the relationship between the location of the maximum area and the section that has the most merged fibers provides a practical method for evaluating the developmental stages of a connection. In other words, the fusion level of a connection can be roughly assessed by directly measuring the area variations within the fused region. Moreover, middle locations of the fused region may give the

best prediction of the fusion level. Regarding the changes observed in cells, according to studies (Korth et al. 2006; Villard et al. 2019), *Ficus* species have adapted to diverse environments by developing physical strategies. The aggregation of calcium oxalate crystals may be considered a physical defense mechanism aimed at improving tissue toughness and forming defense barriers.

Based on the understanding of adaptive growth, the application of self-growing connections extends beyond structural purposes, which include furniture design and agricultural windbreaks. The phenomena and lessons learned from nature can also be applied to other bioinspired and biomimetic designs. For instance, it may improve the fabrication in 3D printing (Schaffner et al. 2018). Additionally, the application of the natural connection can boost the development in bioeconomic.

## Conclusion

In this paper, key findings can be concluded as follows:

1. Within a self-growing connection, the fused region presents a higher density and larger size than the stem region. The increased wood in the fused region is identified as the tension wood with G-layers.
2. The fiber structures of a self-growing connection can be characterized into three groups: the merged fiber bundles connecting the two stems, the deviated fiber bundles, and the normal fiber bundles in each individual stem. Continuous merged fibers are primarily produced in the outer layer passing through the larger cross-angle of a connection. They are the most important component for integrity and structural functions of a self-growing connection.
3. At the periphery of the fused region in a self-growing connection, the interface is mainly made up of bark tissues. In the inner part of a connection, fewer continuous merged fibers are found, mainly organized by parenchyma cells.
4. In the fused region, the location of the largest area can be related to the better fused level, which is represented by more merged fiber bundles. This relation can serve as a practical approach to assess the fusion condition of a connection without influencing its growth.
5. At the cellular level, crystals are observed in the fused region, which might reflect the mechanical stress experienced by the interface.

Future research will focus on the mechanical properties (i.e., strength, stiffness, and loading capacity) of self-growing connections. Moreover, other tree species and fusion technologies can be further investigated.

**Supplementary Information** The online version contains supplementary material available at https://doi.org/10.1007/s00226-024-01622-6.

**Acknowledgements** The authors acknowledge the funding from China Scholarship Council (CSC) and the partial funding support from Deutsche Forschungsgemeinschaft (DFG), entitled Natürlich gewachsene Holzelemente als Basis für tragende Konstruktionen–Statische Analyse und Wachstumssimulation.

(Project Number: 512769030). Support from colleagues Marco Poot and René Hoonhout during the tests is also greatly appreciated.

**Authors' contributions** X. Wang: Conceptualization, Investigation, Data curation, Writing – original draft preparation, Visualization, Formal analysis, Validation. W. Gard: Conceptualization, Supervision, Commentary, Writing—reviewing and editing. Y. Mosleh: Commentary, Writing—reviewing and editing. J.W.G van de Kuilen: Supervision, Conceptualization, Commentary, Writing—reviewing and editing, Project administration, Funding acquisition.

**Data availability** No datasets were generated or analysed during the current study.

## Declarations

**Conflict of interest** The authors declare no competing interests.

**Open Access** This article is licensed under a Creative Commons Attribution 4.0 International License, which permits use, sharing, adaptation, distribution and reproduction in any medium or format, as long as you give appropriate credit to the original author(s) and the source, provide a link to the Creative Commons licence, and indicate if changes were made. The images or other third party material in this article are included in the article's Creative Commons licence, unless indicated otherwise in a credit line to the material. If material is not included in the article's Creative Commons licence and your intended use is not permitted by statutory regulation or exceeds the permitted use, you will need to obtain permission directly from the copyright holder. To view a copy of this licence, visit http://creativecommons.org/licenses/by/4.0/.

## References

Biondi F (2020) From dendrochronology to allometry. Forests 11:146
Braam J (2005) In touch: Plant responses to mechanical stimuli. New Phytol 165:373–389
Brown CL, Sax K (1962) The influence of pressure on the differentiation of secondary tissues. Am J Bot 49:683
Chave J, Coomes D, Jansen S, Lewis SL, Swenson NG, Zanne AE (2009) Towards a worldwide wood economics spectrum. Ecol Lett 12:351–366
Clair B, Alméras T, Yamamoto H, Okuyama T, Sugiyama J (2006) Mechanical behavior of cellulose microfibrils in tension wood, in relation with maturation stress generation. Biophys J 91:1128–1135
Committee IAWA (1989) IAWA list of microscopic features for hardwood identification. IAWA J 10:219–332
Côté WA, Day AC, Timell TE (1969) A contribution to the ultrastructure of tension wood fibers. Wood Sci Technol 3:257–271
Coutand C (2010) Mechanosensing and thigmomorphogenesis, a physiological and biomechanical point of view. Plant Sci 179:168–182
Cramer SM, Goodman JR (1983) Model for stress analysis and strength prediction of lumber. Wood Fiber Sci 79:338–349
Danjon F, Fourcaud T, Bert D (2005) Root architecture and wind-firmness of mature *Pinus pinaster*. New Phytol 168:387–400
Ehrhart T, Brandner R (2018) Rolling shear: Test configurations and properties of some European soft- and hardwood species. Eng Struct 172:554–572
Foley C (2001) A three-dimensional paradigm of fiber orientation in timber. Wood Sci Technol 35:453–465
Fournier M, Dlouhá J, Jaouen G, Almeras T (2013) Integrative biomechanics for tree ecology: beyond wood density and strength. J Exp Bot 64:4793–4815
Freyburger C, Longuetaud F, Mothe F, Constant T, Leban J-M (2009) Measuring wood density by means of X-Ray computer tomography. Ann for Sci 66:804
Hamant O, Moulia B (2016) How do plants read their own shapes? New Phytol 212:333–337
Hamant O, Traas J (2010) The mechanics behind plant development. New Phytol 185:369–385

Hamant O, Heisler MG, Jönsson H, Krupinski P, Uyttewaal M, Bokov P, Corson F, Sahlin P, Boudaoud A, Meyerowitz EM, Couder Y, Traas J (2008) Developmental patterning by mechanical signals in Arabidopsis. Science 322:1650–1655

Jaffe MJ (1980) Morphogenetic responses of plants to mechanical stimuli or stress. Bioscience 30:239–243

Korth KL, Doege SJ, Park SH, Goggin FL, Wang Q, Gomez SK, Liu G, Jia L, Nakata PA (2006) *Medicago truncatula* mutants demonstrate the role of plant calcium oxalate crystals as an effective defense against chewing insects. Plant Physiol 141:188–195

Kouhen M, Dimitrova A, Scippa GS, Trupiano D (2023) The course of mechanical stress: Types, perception, and plant response. Biology 12:217

Kramer EM (2002) A mathematical model of pattern formation in the vascular cambium of trees. J Theor Biol 216:147–158

Kramer EM (2006) Wood grain pattern formation: A brief review. J Plant Growth Regul 25:290–301

Larson PR (1963) Stem form development of forest trees. Forest Sci 9:a0001-42

Lehnebach R, Beyer R, Letort V, Heuret P (2018) The pipe model theory half a century on: A review. Ann Bot 121:773–795

Ludwig F, Schwertfreger H, Storz O (2012) Living systems: Designing growth in Baubotanik. Archit Des 82:82–87

Ludwig F, Middleton W, Gallenmüller F, Rogers P, Speck T (2019) Living bridges using aerial roots of ficus elastic: an interdisciplinary perspective. Sci Rep 9:12226

Mattheck C (1995) Wood - the internal optimization of trees. Arboric J 19:97–110

Mattheck C (1997) Wood - the internal optimization of trees. Springer-Verlag, Berlin Heidelberg New York

Melnyk CW (2017) Plant grafting: Insights into tissue regeneration. Regeneration 4:3–14

Millner EM (1932) Natural grafting in *Hedera* helix. New Phytol 31:2–25

Moulia B, Coutand C, Julien JL (2015) Mechanosensitive control of plant growth: Bearing the load, sensing, transducing, and responding. Front Plant Sci 6:52

Mylo MD, Hesse L, Masselter T, Leupold J, Drozella K, Speck T, Speck O (2021) Morphology and anatomy of branch–branch junctions in opuntia *Ficus* indica and cylindropuntia bigelovii: a comparative study supported by mechanical tissue quantification. Plants 10:2313

Nicoll BC, Ray D (1996) Adaptive growth of tree root systems in response to wind action and site conditions. Tree Physiol 16:891–898

Niklas KJ, Spatz H-CC (2010) Worldwide correlations of mechanical properties and green wood density. Am J Bot 97:1587–1594

Özden S, Slater D, Ennos R (2017) Fracture properties of green wood formed within the forks of hazel (*Corylus avellana* L.). Trees 31:903–917

Ruelle J (2014) The biology of reaction wood. Biol React Wood 14:13–35

Schaffner M, Faber JA, Pianegonda L, Rühs PA, Coulter F, Studart AR (2018) 3D printing of robotic soft actuators with programmable bioinspired architectures. Nat Commun 9:1–9

Scuderi D, Giuffrida F, Toscano S, Romano D (2012) Growth, physiological response, and quality characteristics of weeping fig in response to shading levels and climatic conditions. HortScience 47:1586–1592

Shankar S (2015) Living root bridges: State of knowledge, fundamental research and future application. In: IABSE conference - structural engineering: providing solutions to global challenges. Geneva, Switzerland

Siddiqi TO (1991) Impact of seasonal variation on the structure and activity of vascular cambium in *Ficus religiosa*. IAWA J 12:177–185

Slater D, Ennos AR (2013) Determining the mechanical properties of hazel forks by testing their component parts. Trees Struct Funct 27:1515–1524

Slater D, Ennos R (2015) Interlocking wood grain patterns provide improved wood strength properties in forks of hazel (*Corylus avellana* L.). Arboricultural Journal 37:21–32

Tanaka T, Kawai Y (2013) A new method for nondestructive evaluation of solid wood moisture content based on dual-energy X-ray absorptiometry. Wood Sci Technol 47:1213–1229

Tardif JC, Conciatori F (2015) Microscopic examination of wood: Sample preparation and techniques for light microscopy. Plant Microtechniques and Protocols 20:373–415

Telewski FW, Jaffe MJ (1986) Thigmomorphogenesis: Anatomical, morphological and mechanical analysis of genetically different sibs of *Pinus taeda* in response to mechanical perturbation. Physiol Plant 66:219–226

Valentine HT (1985) Tree-growth models: Derivations employing the pipe-model theory. J Theor Biol 117:579–585
Van de Kuilen J-W, Gard W, Ravenshorst G, Antonelli V, Kovryga A (2017) Shear strength values for soft- and hardwoods. Int Netw Timber Eng Res (INTER) 30:50–061
Villard C, Larbat R, Munakata R, Hehn A (2019) Defence mechanisms of Ficus: Pyramiding strategies to cope with pests and pathogens. Planta 249:617–633
Wang X, Gard W, Borska H, Ursem B, van de Kuilen JWG (2020) Vertical greenery systems: from plants to trees with self-growing interconnections. Eur J Wood Prod 78:1031–1043
Wang X (2024) Build with nature: Biomechanical properties and performance of self-growing connections in interconnected trees. Delft University of Technology
Wardrop AB, Dadswell HE (1948) The nature of reaction wood. Aust J Biol Sci 1:3–16
Zimmermann MH, Wardrop AB, Tomlinson PB (1968) Tension wood in aerial roots of *Ficus benjamina* L. Wood Sci Technol 2:95–104

**Publisher's Note** Springer Nature remains neutral with regard to jurisdictional claims in published maps and institutional affiliations.

## Authors and Affiliations

**Xiuli Wang[1,2] · Wolfgang Gard[1] · Yasmine Mosleh[1] · Jan-Willem van de Kuilen[1,3]**

✉ Xiuli Wang
xiu.wang@fz-juelich.de

Wolfgang Gard
W.F.Gard@tudelft.nl

Yasmine Mosleh
Y.Mosleh@tudelft.nl

Jan-Willem van de Kuilen
vandekuilen@hfm.tum.de

[1] Biobased Structures and Materials, Faculty of Civil Engineering and Geosciences, Delft University of Technology, Delft, The Netherlands

[2] Institute of Bio- and Geosciences, Forschungszentrum Jülich GmbH, IBG-2: Plant Sciences, Jülich, Germany

[3] Wood Technology, Department of Materials Engineering, Technical University of Munich, Munich, Germany